

Modeling and Bounding Low Cost Inertial Sensor Errors

Zhiqiang Xing and Demoz Gebre-Egziabher
University of Minnesota, Twin Cities, Minneapolis, MN

ABSTRACT

This paper presents a methodology for developing models for the post-calibration residual errors of inexpensive inertial sensors in the class normally referred to as "automotive" or "consumer" grade. These sensors are increasingly being used in real-time vehicle navigation and guidance systems. However, manufacturer supplied specification sheets for these sensors seldom provide enough detail to allow constructing the type of error models required for analyzing the performance or assessing the risk associated with navigation and guidance systems. A methodology for generating error models that are accurate and usable in navigation and guidance systems' sensor fusion and risk analysis algorithms is developed and validated. Use of the error models is demonstrated by a simulation in which the performance of an automotive navigation and guidance system is analyzed.

INTRODUCTION

This paper is concerned with developing parametric error models for a class of low cost, solid-state inertial sensors. These sensors are in the quality class normally referred to as "automotive-grade" or "consumer-grade." Recently, there has been a considerable interest in these sensors. One application of these sensors that has attracted some attention is that of enhancing the weak signal tracking ability of Global Navigation Satellite System (GNSS) receivers [1], [2], [3], [4], [5]. In this application the inertial sensors are used to mechanize an Inertial Navigation System (INS) which is tightly or ultra-tightly integrated with a GNSS receiver [6]. Analyzing the performance of these integrated systems requires stochastic models for the output errors of the inertial sensors. In this regard, however, the information provided on specification sheets for these sensors is normally insufficient or incomplete. It

lacks the detail required to construct error models suitable for analyzing the performance of integrated INS/GNSS algorithms. Thus, the user or system integrator of these sensors must construct the required error models.

General methods for constructing inertial sensor error models exist and a representative but non-exhaustive list of works discussing this are [7], [8], [9]. The methods described in [7] and [8] were aimed at developing models for characterizing the output errors of Ring Laser Gyros (RLG) in the quality class normally referred to as "tactical-grade" or "navigation-grade." The methods outlined in [7] and [8] are based on the Allan variance method [10]. The method outlined in [9] also applies the Allan variance method to characterizing gyros with vibrating structure sensing elements.

The methods in [7], [8] and [9] or other similar methods can be applied to automotive- or consumer-grade inertial sensors [12], [13], [14], [15], [16]. However, this is not an efficient approach to generating error models for several reasons. First, these sensors are normally used in a setting where they are integrated with an aiding sensor and relied on in a stand-alone fashion only for brief moments. Thus, the detailed modeling of long term error characteristics along the lines of [7], [8] and [9] is unnecessary. Second, they generate high-order error models (*i.e.*, error models with many terms). While these error terms may be helpful in characterizing the sensor outputs in a laboratory or manufacturing setting, they may not be separately observable on-line in an estimator. Using these high-order error models can have deleterious effects on INS/GNSS filter observability. Finally, these methods generate frequency domain description for some of the output error modes which are difficult to recast into time domain models (e.g., flicker noise).

It is the thesis of this paper that the output errors for these sensors can adequately and conservatively be modeled

using a four parameter error model; one scale factor error term and a three parameter bias error model. The three-parameter bias model has two terms which capture the effect of correlated and uncorrelated errors, respectively. A methodology for estimating the three parameters that define the error model from sensor output data is also presented. In cases where the error models are used in applications such as [18] where navigation risk analysis needs to be performed (using, for example, the approaches given in [19], [20]), the error models can be tuned to generate over-bounds.

Accordingly, the remainder of this paper is organized as follows: In the section that follows, the general structure of the error model is proposed. Then the use of the Allan variance for modeling the output bias of these sensors is examined. This is followed by a description of a proposed methodology for determining error model parameters. Simulation and experimental data highlighting the modeling approach is then presented. Summary and concluding remarks will close the paper.

ERROR MODEL STRUCTURE

In general, inertial sensor output errors can be divided into two parts; deterministic errors and random errors [9]. The deterministic component accounts for output errors due to external factors such as temperature or acceleration. It is possible to identify these external factors and develop an accurate model describing their effects on the sensor errors. If one compensates for the output errors caused by these external factors—using a look-up table, for example—their contribution to the output error is removed[11]. It is impossible, however, to identify all of these external factors. Even if it were possible to identify them, it would be impossible to *completely* remove the errors caused by them, since there will be a residual error (albeit small) left after compensation. For modeling purposes these residuals are combined with the other random effects. The focus of this paper is developing models for the combined residual and random errors. It should be noted that, the resulting error models are stochastic in nature and, thus, cannot be used to improve the sensor output. Instead, they are used to provide a statistical bound on the expected output errors caused by these un-modeled or post-calibration residual effects.

If we use y to denote sensor outputs, then the general post calibration model proposed to describe these errors has the following form:

$$y_m = (1 + k)y_t + b(t). \quad (1)$$

In Equation 1, y_m is the sensor's measured output and y_t is the true value of the quantity that the sensor is measuring.

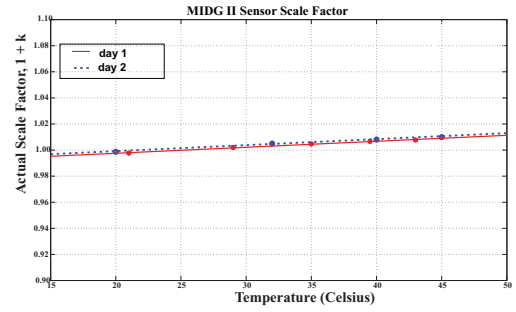


Fig. 1: Scale Factor versus Temperature for an Automotive-Grade Rate Gyro Used in the MIDG II Inertial Navigation System [34]

Stated differently, y_m is the sensors representation of y_t . The true value y_t is corrupted by a scale factor error, k , and a bias, $b(t)$. In general, the bias is time varying. Since we are interested in modeling post calibration errors, $b(t)$ can be thought of as the residual output of the sensor when no input is applied. Thus, it can be measured or observed when the sensor is static.

For these low cost inertial sensors, we are more interested in modeling the stochastic nature of the residual $b(t)$ than the scale factor error k . This is because, the stochastic variations of the scale factor error is small and its effect is minimal in comparison to the effects of the variations in $b(t)$. As an example of this consider the experimental data shown in Figure 1. This shows estimates of the combined $1 + k$ as a function of temperature for an automotive-grade rate gyro. The data was collected from a rate table inside a temperature-controlled environmental chamber. The data clearly shows that k is a function of temperature. However, the variability of k from one day to the next is very small. This implies that the change of k over a small time window when these sensors are being used in a stand-alone fashion is going to be small. Thus, a stochastic error model for the scale factor is unnecessary. This does not imply an estimator used for blending the output from these sensors with a GNSS receiver should not include a state for scale factor error. What it implies is that the scale factor can be modeled adequately as a random constant. The situation with the bias term, however, is different. If we divide the bias errors into time varying and time-invariant components, then without a loss of generality we can assume $b(t)$ has the following form:

$$b(t) = b_0 + b_R(t). \quad (2)$$

The term b_0 represents a *constant* null-shift. Its value is sometimes listed on data sheets for inertial sensors and is referred to as the "turn-on to turn-off" bias. It is relatively easy to estimate. The term $b_R(t)$ represents the random bias drift, or the residual of the bias after calibration. The term "drift" implies that it is time-varying. Since b_0

Error Mechanism	Allan Variance Slope
Wide-Band Noise	$-\frac{1}{2}$
Quantization Noise	-1
Exponentially Correlated Noise (First Order Gauss-Markov Process)	$[-\frac{1}{2}, +\frac{1}{2}]$ (depends on value of τ_a)
Rate Random Walk	$+\frac{1}{2}$
Linear Rate Ramp	$+1$
Flicker Noise	0

TABLE I: Summary of Standard Error Sources and their Respective Allan Variance Slopes

is relative easy to determine, the focus in this paper is primarily associated with characterizing $b_R(t)$ for low cost inertial sensors.

A tool that is frequently used in the modeling of inertial sensor errors is the Allan variance. While we will also use the Allan variance here, we note that care should be taken when applying it to low cost inertial sensor error modeling. In the section that follows we will discuss this aspect of the Allan variance.

ALLAN VARIANCE: OVERVIEW AND LIMITATIONS

The Allan variance of a random process can be viewed as the time domain equivalent of its Power Spectral Density (PSD). However, instead of power as a function of frequency it gives the Allan variance β^2 (to be defined shortly and mathematically related to the PSD) as a function of averaging time, τ_a . The theory and details of the Allan variance method can be found in the seminal work on the topic documented in [10] as well as applications of the method to inertial sensor error modeling given in [9], [7] and [8].

From [7] and [8] we know that the Allan variance, $\beta^2(\tau_a)$, of a time series of gyro data collected over a time interval T seconds long, is related to the PSD of the output noise $S(f)$ by the following equation (where f is frequency):

$$\beta^2(\tau_a) = \frac{4}{\pi\tau_a} \int_0^\infty S\left(\frac{u}{\pi T}\right) \frac{\sin^4 u}{u} du. \quad (3)$$

When β versus τ_a are plotted on a log-log plot, random processes corrupting the rate gyro output or present in the post-calibration residuals will appear as lines with the slopes given in Table I. Prior work in modeling low cost rate gyros which relied on Allan variance analysis assumed that different error sources were reasonably separated in frequency such that each error mechanism had a unique slope. If this assumption is valid (as it is with high quality rate gyros), then the various error mechanisms can be identified from the Allan variance slopes where the magnitude of each error mechanism is determined by line-

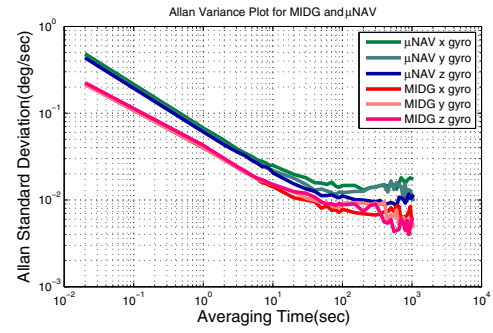


Fig. 2: Allan Variance Plots for Typical Low Cost Rate Gyros—Crossbow μ Nav [33] and the MIDG II Inertial Navigation System [34].

fitting as described in [8]. However, when we examine the Allan variance plots for low cost sensors we find that the correlated errors have slopes that are not necessarily equal to any *one* of the error mechanisms listed in Table I. Figure 2 shows this clearly. This figure shows the Allan variance for two different brands of low cost gyros. The data used to construct the Allan Variance plots is the 3-hour static output data sampled at 50 Hz. While the Allan variance for all these gyros exhibits a $-1/2$ slope for small τ_a , for larger τ_a values the slopes are seen to increase gradually to zero and sometimes positive. From this observation it can be concluded that a stochastic model for $b_R(t)$ would be the superposition of white noise and correlated noises.

To see the structure of the correlated noise more clearly, the Allan variance for one μ Nav gyro is shown in Figure 3. The correlated and uncorrelated parts of the output errors are separated using a method described later in the paper. The uncorrelated and correlated noises are plotted separately as shown in Figure 3. It can be seen that the correlated noise exhibits a slowly changing and slightly positive slope. It does not match any of the slopes identified in Table I.

Prior work associated with low cost inertial sensors has typically modeled the error associated with the zero-slope part of the Allan variance as a constant bias and in some instances, unfortunately, labeled it with the moniker "bias instability". In some instances, it was modeled as a combination of a constant bias and a random walk [12], [13], [14], [15], [16]. However, a zero-slope Allan variance corresponds to a flicker noise process which is difficult to model in the time-domain with finite-order state model. It is sometimes approximated as the combination of several exponentially correlated noise terms. Based on these observations, we note that $b_R(t)$ is the superposition of a wide band noise process which is the dominant error source for small τ_a and several correlated stochastic processes which become dominant for larger values of τ_a .

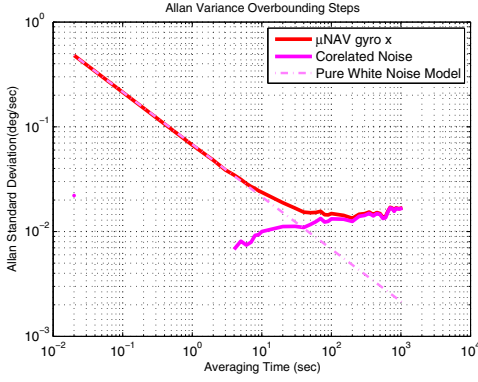


Fig. 3: Allan Variance Plots for Crossbow μ Nav Gyro showing White Noise and Correlated Noise.

Thus, it is reasonable to model post-calibration residual errors as:

$$b_R(t) = b_w(t) + \sum_{i=1}^N b_i(t), \quad (4)$$

where $b_w(t)$ is a wide band noise process and $b_i(t)$ is the i^{th} correlated time domain error process. As noted earlier, however, the objective of this paper is to develop an error model which is a compromise between accuracy and usability. If N is large, including all N correlated error terms would negatively affect usability. Reducing the number of correlated error terms included in the model enhances usability but at the cost of accuracy. In addition, noting that these low-cost sensors are normally used in a setting where they are integrated with an aiding sensor and relied on in a stand-alone fashion only for brief moments, the detailed modeling of long term error characteristics (the effect of random walk usually show up in the averaging time range above several thousands seconds) is unnecessary.

As a compromise between usability and accuracy, we propose retaining a single correlated error term (denoted $b_1(t)$) with tuning parameters that can be adjusted to approximate and overbound the Allan Variance plot of correlated noise in a averaging time range we are interested (for example, 5-1000 seconds). The proposed form for $b_1(t)$ will be an exponentially correlated or first order Gauss-Markov process where the variance $\sigma_{b_1}^2$ and time constant τ_{b_1} are the tuning parameters. Before we justify the reasonableness of replacing $\sum_{i=1}^N b_i(t)$ in Equation 4 with a single Gauss-Markov process $b_1(t)$, we note that the proposed form of $b_R(t)$ is $b_R(t) = b_w(t) + b_1(t)$ and the resulting total error model for the residual $b(t)$ is:

$$b(t) = b_0 + b_w(t) + b_1(t). \quad (5)$$

This total error model is schematically depicted in Figure 4 where the physical meaning of each of the terms in Equation 5 is shown graphically.

Replacing $\sum_{i=1}^N b_i(t)$ with $b_1(t)$

The first order Gauss-Markov process $b_1(t)$ can be thought of as the output of a first order low-pass filter with cutoff frequency f_c of $1/2\pi\tau_{b_1}$. The input to the filter is a white noise process w_{b_1} with a PSD of $Q_{w_{b_1}} = 2\sigma_{b_1}^2/\tau_{b_1}$ where $\sigma_{b_1}^2$ is the variance of $b_1(t)$. The PSD of this process is given by [35], [36]:

$$S_{b_1}(f) = \frac{Q_{w_{b_1}} \tau_{b_1}^2}{1 + (2\pi\tau_{b_1}f)^2} \quad (6)$$

where τ_{b_1} is the time constant of the process and $Q_{w_{b_1}}$ is the constant PSD of the driving white noise w_{b_1} . Equivalently, a time domain description of the process can be written as the following first order stochastic differential equation:

$$\dot{b}_1(t) = -\frac{1}{\tau_{b_1}}b_1(t) + w_{b_1}. \quad (7)$$

The variable τ_{b_1} is the time constant (or correlation time) and w_{b_1} is the driving white process noise. The mathematical equation and Allan variance plot of this process is referred to [24]. It is useful to know the limiting case of the first order Gauss-Markov process in Allan variance plot.

When τ_a is much smaller than the correlation time τ_{b_1} , the limit is a random walk process with driving process having a PSD of $Q_{w_{b_1}}$:

$$\beta^2(\tau_a) = \frac{Q_{w_{b_1}}}{3} \tau_a. \quad (8)$$

When τ_a is much larger than the correlation time τ_{b_1} , the limit is a white noise process with PSD $Q_{w_{b_1}} \tau_{b_1}^2$:

$$\beta^2(\tau_a) = \frac{Q_{w_{b_1}} \tau_{b_1}^2}{\tau_a}. \quad (9)$$

Compared with a random walk model (as was used in [25]) we have more flexibility when using a first order Gauss-Markov process because we have two parameters with which we can tune the model. We can have a tighter bound using Gauss-Markov process model other than random walk model.

In summary, a reasonable unified error model for the output errors of these inexpensive inertial sensors is one that has the form shown schematically in Figure 4. As shown in this figure, the bias $b(t)$ consists of a time invariant and time-varying components. The time invariant or constant part is called a null-shift and from Figure 4 it is clear why that is the case; it represents the shift of the output error away from zero. The time varying component consists of a wide band noise component and a correlated component. A model for the correlated part that can bound a reasonably wide variety of error mechanism is the first order Gauss-Markov process.

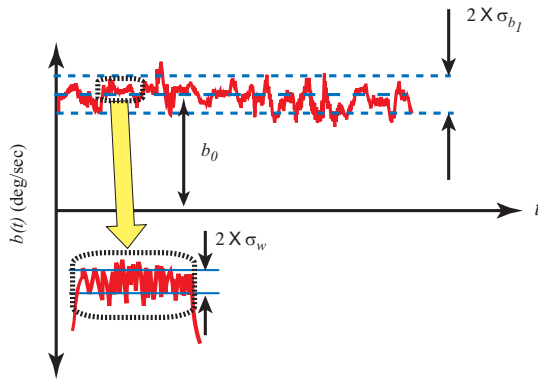


Fig. 4: A Schematic of the General Error Model Proposed In this Paper

ESTIMATING MODEL PARAMETER VALUES

In order to complete the mathematical description of $b(t)$, numerical values for its various components must be determined. The numerical values that must be determined are the following: (1) The null-shift b_0 and its variance $\sigma_{b_0}^2$. (2) The power spectral density of b_w , Q_w , or the variance of its discrete realization, $\sigma_{b_w}^2$. (3) The variance of $b_1(t)$, $\sigma_{b_1}^2$. (4) The correlation time of $b_1(t)$, τ_{b_1} .

Determining Numerical Values for $\sigma_{b_0}^2$

The term b_0 is a null-shift and once a gyro is powered-on, its value remains relatively constant. Subsequently, if the gyro is powered-off then powered-on again, the new value of b_0 may be different. It will remain at this new constant as long as the gyro remains powered-on. This suggests that b_0 can be modeled as a random constant. The statistics of b_0 can be determined from an ensemble of experiments which consist of turning on the gyro, recording $b(t)$ for period of time on the order of tens of minutes and taking the mean of this data. Since the random constant model assumed for b_0 is non-ergodic and because both the wide band noise and first order Gauss-Markov processes are zero mean, the value of b_0 for each on/off cycle is the time average of $b(t)$. The value for b_0 computed for many such on-off cycles can be used to generate a description of the statistics for b_0 .

The only question that remains is how many on/off cycles are required to accurately characterize $\sigma_{b_0}^2$? This question may be answered by noting how knowledge of b_0 and $\sigma_{b_0}^2$ are used in navigation, guidance and control applications. In many multi-sensor system applications such as those described in [21], [2], [1] and [28] the combination $b_0 + b_1(t)$ is continually estimated (in real time) using an observer. Thus, we do not need to know its value *a*

priori. The primary use of $\sigma_{b_0}^2$ is for establishing initial conditions on state covariance matrices of multi-sensor fusion system algorithms such as the Extended Kalman Filter. Since these algorithms refine the state covariance estimates continually, a precise knowledge of it may not be required.

Determining Numerical Values for Q_w or $\sigma_{b_w}^2$

The wide band noise component of the error model, $b_w(t)$, is a random process which can be described in one of two ways. If we elect to use a continuous time description of the process, then it can be characterized by its PSD, Q_w . On the other hand, if we elect to use a discrete time description of the process, then the variance of discrete samples of $b_w(t)$ can be used. In the latter case, we are modeling $b_w(t)$ as a band limited white noise process or a white sequence [35]. Since many sensors' outputs are digital and the sensor fusion algorithms that use them are discrete time systems, we will use the latter description of $b_w(t)$.

The variance of the discrete time description of b_w , σ_{b_w} , can be obtained by reading out the Allan standard deviation value when τ_a is equal to T_s . However, considering the variation in constructing Allan variance, it is better to draw a line with a slope of $-1/2$ in log-log plot to overbound the Allan variance plot for small τ_a (for example, less than 5 sec), and reading out the Allan standard deviation value of the overbounding line when τ_a is equal to T_s .

Since the method of computing $\sigma_{b_w}^2$ discussed above assumes that $b_w(t)$ is a white noise sequence (band limited) and not a white noise process, it is valid to ask whether this assumption is justified. As shown in [21] this assumption is valid because the output of many low cost rate gyros is digital and has gone through significant processing that the end user cannot control. Thus, although b_w may be white noise process at the sensing element internal to the sensor, the output which follows internal sampling and filtering will have a power spectrum that is clearly band limited. In the case that the output is not digital, care must be taken and the sensor sampling rate must be taken into account before using the above method to estimate $\sigma_{b_w}^2$.

Determining τ_{b_1} and $\sigma_{b_1}^2$

Since $b_1(t)$ is modeled as a first order Gauss-Markov process, we can completely describe it by two parameters: its correlation time, τ_{b_1} , and variance, $\sigma_{b_1}^2$. In theory, the variance and time constant of a first order Gauss-Markov process can be determined from a plot of the process' autocorrelation function, $R_{b_1}(t_1, t_2)$. In practice, however,

this is difficult. This is because actual output data from low cost rate gyros is a combination of wide band noise and a correlated process. Furthermore, the magnitude of the wide band noise is much larger than the magnitude of the correlated noise. As such, it is difficult to separately identify the correlated process from an autocorrelation plot constructed using gyro output data directly without any pre-processing.

Another difficulty arises from the fact that in the modeling approach proposed here, we are replacing $\sum_{i=1}^N b_i(t)$ with $b_1(t)$. Since $\sum_{i=1}^N b_i(t)$ may be the superposition of multiple Gauss-Markov processes and potentially other random processes, it may not be possible to fit a single Gauss-Markov process to the sampled gyro data.

In view of this latter point, we reiterate that in the approach proposed here, the first order Gauss-Markov process is used to overbound the output errors and not necessarily model them *exactly*. With these issues in view, in this paper we propose the following simple Allan variance based procedure for getting initial estimates of τ_{b_1} and $\sigma_{b_1}^2$. First, generate an Allan variance plot from the sampled $b(t)$ data and plot Allan variance of the correlated noise by subtracting white noise from total Allan variance. This is done using the following equation:

$$\beta_{\text{Total}}^2(\tau_a) = \beta_w^2(\tau_a) + \beta_{b_1}^2(\tau_a). \quad (10)$$

Next, compute Q_{wb_1} which is the constant PSD of the driving white noise. When τ_a is small compared with τ_{b_1} , the Allan Variance of a first order Gauss-Markov process is what we call the *limit line*. It has a slope of +1/2 in a log-log plot. The position of this line is affected by Q_{wb_1} only. We want this limit line to overbound the correlated noise on a log-log plot.

Now we are in a position to generate an initial estimate of $\sigma_{b_1}^2$. To do this, we note that the variance of the uncorrelated (wide band) noise is normally very large compared to the variance of the correlated noise. Thus, estimating the variance of correlated noise directly from the raw output data is challenging. But, we can pass this data through a low pass filter (e.g., 1 Hz averaging) to mitigate the effect of the wide band noise. During this filtering, the uncorrelated noise will still stay uncorrelated with a variance of σ_{bw}^2/f_s . Furthermore, the correlated noise will remain almost unaltered since its correlation time is in a range much larger than 1 second. The total variance of the filtered data will be the sum of the filtered wide band noise and correlated noise. Thus,

$$\sigma_{b_1}^2 = \sigma_{\text{total}}^2 - \sigma_{bw}^2/f_s \quad (11)$$

Using this value of σ_{b_1} and the previously estimated value of Q_{wb_1} we can plot the exponentially correlated noise on an Allan variance chart. This plot can now be tuned (i.e.,

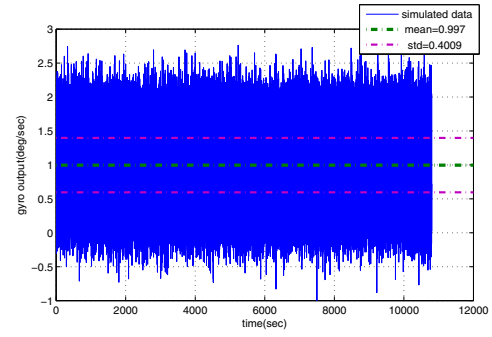


Fig. 5: Simulated Gyro Output Data.

moved) to get an overbound for σ_{b_1} . Finally, we determine τ_{b_1} from the following relation:

$$\tau_{b_1} = \frac{2\sigma_{b_1}^2}{Q_{wb_1}} \quad (12)$$

DEMONSTRATIVE EXAMPLE OF ERROR MODELING

In order to demonstrate how one can construct rate gyro error models, we will present an illustrative example where we use a simulated rate gyro output and apply the methodology outlined above. The output is from a rate gyro that is static (i.e. y_t in Equation 1 is zero). The output of the gyro is corrupted by a null-shift, wide band and correlated errors. The null shift b_0 is equal to 1 deg/sec. The wide band noise standard deviation σ_w is equal to 0.40 deg/sec. The correlated error is modeled as the superposition of two random processes. The first one is a first order Gauss-Markov process with $\sigma_{b_1} = 0.02$ deg/sec and correlation time $\tau = 150$ sec. The second one is also a first order Gauss-Markov process with $\sigma_{b_1} = 0.015$ deg/sec and correlation time $\tau = 1000$ sec. A long correlation time was selected for this process to represent residuals in the thermal modeling of the gyros. A 3 hour time series of this gyro's output is simulated and the data is sampled at 50 Hz to be used in the subsequent modeling exercise. Figure 5 shows this 3 hour simulated time series.

Determining b_0 and σ_{bw}

It is straight forward to obtain b_0 as it can be computed by averaging the long term data or using an estimator that is part of the navigation system that employs the sensor. From a simple averaging of the data used to construct Figure 5 yields the value of $b_0 = 0.997$ deg/sec.

To find σ_{bw} , we construct an Allan variance plot as shown in Figure 6. Note that σ_{bw} is equal to the value of the Allan

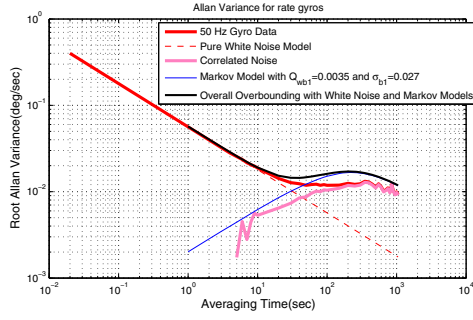


Fig. 6: Overbounding Procedure for Simulated Gyro Data.

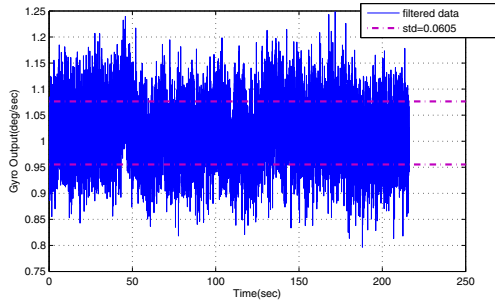


Fig. 7: Simulated Gyro Time Series (Averaged Every One Second) .

variance when $\tau_a = T_s$ where T_s is the signal sampling rate. From Figure 6 we see that the value of the Allan variance at $\tau_a = T_s$ is 0.402 deg/sec which is near the simulated value of σ_w .

Determining σ_{b_1} and τ_{b_1}

Next we plot the Allan variance of the correlated noise by subtracting the white noise from the total Allan variance as described earlier. If we do this, we find that $Q_{wb_1} = 0.0035^2(\text{deg/sec}^{\frac{3}{2}})^2$. We then filter $b_R(t)$ by binning the data into 1 second windows and averaging (i.e., decimate the data to 1 Hz). This is shown in Figure 7. The variance of the filtered data is seen to be equal to 0.0605^2 deg/sec for this example. We need to subtract filtered white noise variance from this. The white noise variance is equal $\sigma_{b_w}^2/f_s = 0.0032(\text{deg/sec})^2$. After this subtraction the remaining power of the correlated process is 0.0215^2 (deg/sec)² and the estimated σ_{b_1} is 0.0215 deg/sec. We can stop here or tune the model a little more to get an overbounding value for σ_{b_1} . If we do this, we get $\sigma_{b_1} = 0.027(\text{deg/sec})$ and an associated time constant τ_{b_1} of 119 sec.

In the above example we sampled the data at a frequency

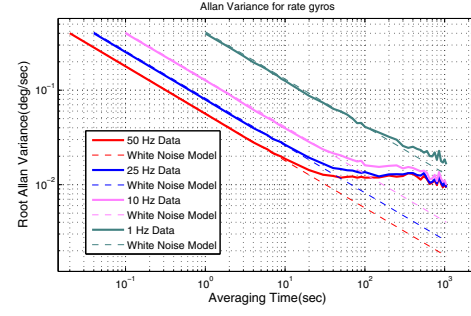


Fig. 8: Allan Variance Plots of Simulated Data for Different Sampling Frequencies .

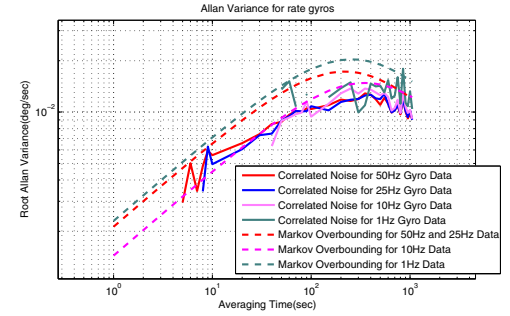


Fig. 9: Allan Variance Overbounding of Simulated Data for Different Sampling Frequencies .

of 50 Hz. In practice, we may use different sampling frequencies. The method developed will still work for various sampling rates. This can be seen in the Allan variance plots and corresponding white noise models shown in Figure 8. The estimate for the resulting error models using different sampling frequency data are summarized in Table II. We note that the correlation time estimates are poor relative to the estimates for σ_{b_w} and σ_{b_1} . This is not surprising because: (1) There is a second correlated process buried in the noise with a longer correlation time. We have ignored this second process or do not know of its presence. (2) As discussed in [37] estimates of τ are very sensitive to noise. However, as we will show next, this is not a concern because the model is just a starting point for a model that will ultimately be used in navigation and guidance system.

f	b_w	$b_1(t)$	
	σ_{b_w}	τ_{b_1}	σ_{b_1}
50 Hz	0.402deg/sec	119 sec	0.027 deg/sec
25 Hz	0.41deg/sec	119 sec	0.027 deg/sec
10 Hz	0.41deg/sec	184 sec	0.024 deg/sec
1 Hz	0.41deg/sec	136 sec	0.033 deg/sec

TABLE II: Parameters for Rate Gyro Output Error Models.

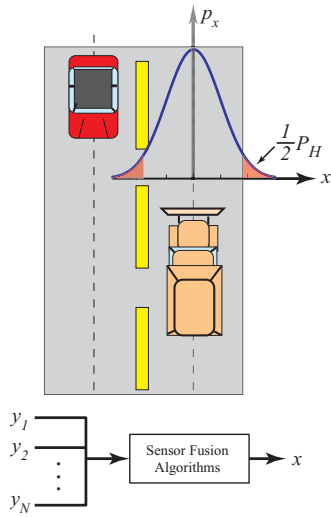


Fig. 10: An Unmanned Ground Vehicle(Left) In Operation.

UGV DEAD RECKONING SYSTEM ERROR BOUNDING

As case study let us consider the automotive guidance and control problem discussed in [30], [31], [32] and depicted in Figure 10. It is the navigation and guidance problem for a large snow plow in low visibility conditions. The vehicle operates in a lane of width d and the state variable x is its deviation from the centerline of the lane. As shown in the block diagram in Figure 10, x is estimated in real time by fusing the outputs y_i (where $i = 1, 2, \dots, N$) of many sensors including rate gyros. The dynamic model for this problem has three states. These states are the lateral position (x), the heading angle (ψ) and distance traveled along track (s). Mathematically, this dynamic model is written as:

$$\dot{\mathbf{z}} = \begin{bmatrix} \dot{s} \\ \dot{x} \\ \dot{\psi} \end{bmatrix} = \mathbf{f}(\mathbf{z}) = \begin{bmatrix} V \cos(\psi) \\ V \sin(\psi) \\ r \end{bmatrix}. \quad (13)$$

Since this is a problem where navigation and guidance errors have safety-of-life implications, we are interested in bounding the risk. For example, we may want to quantify the risk that an undetected sensor error will cause a hazardous condition like the case where the snowplow is in the wrong lane but the sensor fusion algorithms generate an estimate of x indicating otherwise. The probability of such an occurrence is denoted P_H (subscript "H" for "Hazard") and is equal to:

$$\begin{aligned} P_H &= P\{x > d \cup x < -d\} \\ &= \int_{-\infty}^{-d} p_x dx + \int_d^{+\infty} p_x dx. \end{aligned} \quad (14)$$

This risk is equal to the shaded area under the probability density function for x shown in Figure 10. Precisely or conservatively quantifying P_H requires error models for the sensors used in the navigation system. In this case we assume that the navigation system only uses two sensors; a Doppler radar for sensing speed and a rate gyro for sensing heading. For simplicity and clarity, we assume that the vehicle is heading north and uses an error-free Doppler radar measuring a constant speed of 60 km/hr. The output of the rate gyros is r and is integrated to yield heading, ψ . We further assume the output errors on the rate gyro are equal to the errors used in the previous modeling example with the only difference that b_0 has already been estimated and removed from the gyro outputs.

To perform a covariance analysis, we must linearize the nonlinear model given by Equation 13 and augment the state vector with the gyro bias, b_1 , as follows:

$$\delta \mathbf{z} = \begin{bmatrix} \delta s \\ \delta x \\ \delta \psi \\ b_1 \end{bmatrix} \quad (15)$$

The equation that governs the propagation of the state errors in time is then given by:

$$d(\delta \mathbf{z})/dt = \mathbf{F} \delta \mathbf{z} + \mathbf{G} \mathbf{w} \quad (16)$$

where,

$$\mathbf{F} = \begin{bmatrix} 0 & 0 & -\sin(\psi)V & 0 \\ 0 & 0 & \cos(\psi) & 0 \\ 0 & 0 & 0 & 1 \\ 0 & 0 & 0 & -\frac{1}{\tau} \end{bmatrix} \quad (17)$$

$$\mathbf{G} = \begin{bmatrix} 0 & 0 \\ 0 & 0 \\ 1 & 0 \\ 0 & 1 \end{bmatrix} \quad (18)$$

$$\mathbf{w} = \begin{bmatrix} b_w \\ w_{b_1} \end{bmatrix}. \quad (19)$$

Denoting the discrete equivalent of \mathbf{F} as Φ , the covariance propagation for the navigation state errors will be governed by:

$$\mathbf{P}_k = \mathcal{E}\{\delta \mathbf{z}_k \delta \mathbf{z}_k^T\} \quad (20)$$

$$= \Phi_{k-1} \mathbf{P}_{k-1} \Phi_{k-1}^T + \Gamma_{k-1} \quad (21)$$

where Γ_{k-1} is the discrete equivalent $\mathbf{G} \mathbf{Q}_w \mathbf{G}^T$ and \mathbf{Q}_w is the power spectral density matrix of \mathbf{w} .

In what follows we perform a covariance analysis to compare the fidelity of the error estimates using the following two models: (1) A model consisting of b_w only as proposed in [22] and (2) A model consisting of b_w and b_1 as developed in this paper. The results of this analysis are shown in Figures 12, 13, 14 and 15. We use data collected from the Crossbow μ Nav Inertial Measurement

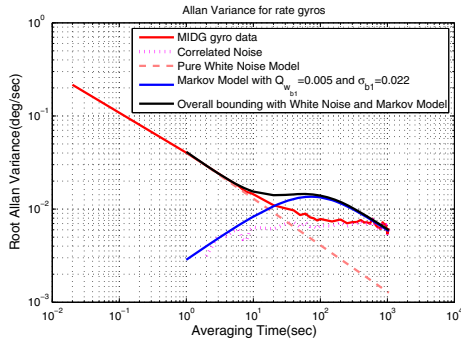


Fig. 11: MIDG Overbounding Procedure.

Models	b_w	$b_1(t)$	
	σ_{b_w}	τ_{b_1}	σ_{b_1}
μ NAV 1	0.482 deg/sec	-	-
μ NAV 2	0.482 deg/sec	92 sec	0.042 deg/sec
MIDG 1	0.286 deg/sec	-	-
MIDG 2	0.286 deg/sec	39 sec	0.022 deg/sec

TABLE III: Parameters for Rate Gyro Output Error Models.

Unit (IMU) [33] and the Microbotics MIDG II Inertial Measurement Unit (IMU) [34]. The root Allan variance for the rate gyros in these IMUs and the procedure to estimate the models parameter are shown in Figure 3 and Figure 11. The estimate for the resulting error models are summarized in Table III.

Although the simple wide band noise model can bound the error in the first few seconds, it loses its bounding ability afterwards. If we add a first order Gauss-Markov model with tuned parameters to account for correlated part, we can bound the estimation error tightly in any time span we are interested. In turn, this means we can have an evaluation of Equation 14 which is conservative and accurate.

CONCLUSION

This paper developed and validated unified mathematical models for the behavior of the post calibration residual errors of a class of low cost inertial sensors. The model developed is unified in that it is a single model which can be used to capture or bound the behavior of various output errors normally seen in this class of inertial sensors. This paper also shows how these models can be tuned to bound the output errors of navigation, guidance and control systems that use these sensors. A covariance analysis associated with a vehicle navigation and guidance problem which uses these gyros is presented. By comparing the analysis results to experimental data, it has been shown the

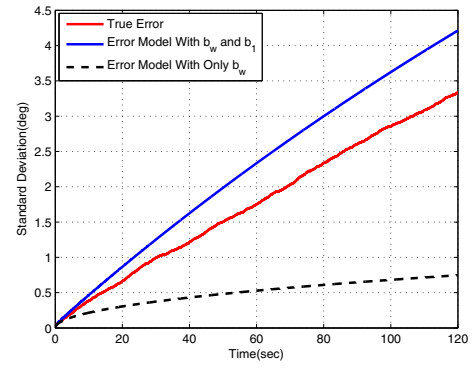


Fig. 12: Navigation Simulation And Actual μ NAV Data Comparison. Heading Errors.

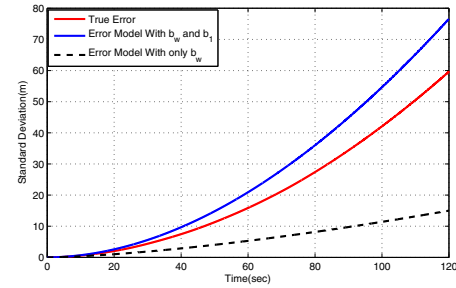


Fig. 13: Navigation Simulation And Actual μ NAV Data Comparison. Position (Cross Track) Errors.

prediction of the performance of navigation and guidance systems can be bounded conservatively and tightly. More importantly, however, these error models are amenable for use in risk analysis of vehicle navigation and guidance systems.

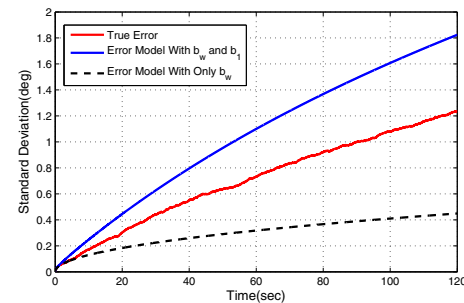


Fig. 14: Navigation Simulation And Actual MIDG Data Comparison. Heading Errors.

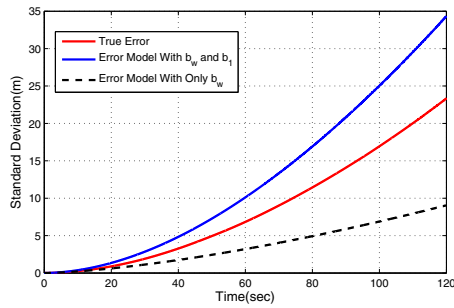


Fig. 15: Navigation Simulation And Actual MIDG Data Comparison. Position (Cross Track) Errors.

ACKNOWLEDGEMENTS

The authors gratefully acknowledge the support of the Intelligent Transportation Institute (ITS) Institute at the University of Minnesota for the grant that supported this work. The views expressed in this paper, however, belong to the authors alone and do not necessarily represent the position of any other organization or person.

References

- [1] Gao, G. and G. Lachapelle, "INS-Assisted High Sensitivity GPS Receivers For Degraded Signal Navigation," *Proceedings of the ION-GNSS 2006 Conference*, Ft. Worth, TX, 2006.
- [2] Petovello, M. and G. Lachapelle, "Comparison of Vector-Based Software Receiver Implementations With Application to Ultra-Tight GPS/INS Integration," *Proceedings of the ION-GNSS 2006 Conference*, Ft. Worth, TX, 2006.
- [3] Soloviev, A., F. Van Graas, and A. Gunawardena, "Implementation Of Deeply Integrated GPS/Low-Cost IMU For Acquisition And Tracking Of Low CNR GPS Signals", *Proceedings of ION National Technical Meeting 2004*, Anaheim, CA., pp. 611-622, 2004.
- [4] Gunawardena, A., A. Soloviev, F. Van Graas, and A. Gunawardena, "Implementation Of Deeply Integrated GPS/Low-Cost IMU For Acquisition And Tracking Of Low CNR GPS Signals", *Proceedings of ION National Technical Meeting 2004*, Anaheim, CA., pp. 611-622, 2004.
- [5] Kreye, C., Eissfeller, B. and Winkel, J. O., "Improvements of GNSS Receiver Performance Using Deeply Coupled INS Measurements," *Proceeding of the Institute of Navigation GPS Conference (ION-GPS) 2000*, Salt Lake City, UT. pp. 844-854.
- [6] Gebre-Egziabher, D., "GNSS Solutions: Variations of GNSS/INS Integration," *Inside GNSS*, Vol 2., No. 1, January/February 2007. pp. 28-33.
- [7] Tehrani, M. M., "Ring Laser Gyro Data Analysis with Cluster Sampling Technique," *Proceedings of SPIE*, Vol. 42, No. 2. pp. 207-220.
- [8] Ng, L. C., D. J. Pines, "Characterization of Ring Laser Gyro Performance Using the Allan-Variance Method," *AIAA Journal of Guidance Control and Navigation*, Vol. 20, No. 1. July-August 1984. pp. 211-213.
- [9] IEEE Gyro and Accelerometer Panel, *Draft Standard Specifications Format Guide and Test Procedure for Coriolis Vibratory Gyros*, Draft Standard.
- [10] Allan, D. W., "Statistics of Atomic Frequency Standards," *Proceedings of the IEEE*, Vol. 54, No. 2. Feb. 1966. pp. 221-230.
- [11] Jose A. Rios, Elecia White, *Low Cost Solid State GPS/INS Package*, www.xbow.com
- [12] Naser El-Sheimy, Haiying Hou, Xiaoji Niu, *Analysis and Modeling of Inertial Sensors Using Allan Variance*, IEEE Transactions on Instrumentation and Measurement, VOL 57, NO 1, Jan 2008
- [13] Angelo Maria Sabatini, *A Wavelet-based Bootstrap Method Applied to Inertial Sensor Stochastic Error Modelling Using the Allan Variance*, Institute of Physics Publishing, Measurement Science and Technology, 17,(2006) 2980-2988
- [14] Xiaoji Niu, Sameh Nassar, and Naser El-Sheimy, *An Accurate Land-Vehicle MEMS IMU/GPS Navigation System Using 3D Auxiliary Velocity Updates*, Journal of Navigation, Vol. 54 No. 3, 2007
- [15] Hyunseok Kim, Jang Gyu Lee, Chan Gook Park, *Performance Improvement of GPS/INS Integrated System Using Allan Variance Analysis*, The 2004 International Symposium on GPSS/GPS
- [16] Yudan Yi, *On Improving the Accuracy and reliability of GPS/INS-Based Direct Sensor Georeferencing*, PhD Thesis, 2007, The Ohio State University
- [17] Gebre-Egziabher, D., Elkaim, G. H., Powell, J. D., and Parkinson, B. W., "A Gyro-Free Quaternion Based Attitude Determination System Suitable for Implementation Using Low-Cost Sensors," *Proceedings of the IEEE PLANS 2002*, San Diego, CA, 2002. pp 185 - 192.
- [18] Weibel, R. E. and R. J. Hansman, "An Integrated Approach to Evaluation of Risk Mitigation Measures for UAV Operational Concepts in the NAS," AIAA Paper AIAA-2005-6957. *Proceedings of the AIAA 4th Infotech Conference*. September 2005. Arlington, VA.
- [19] Rife, J. H. and D. Gebre-Egziabher, "Symmetric Overbounding of Correlated Errors," *Proceedings of ION-GNSS 2006*, Ft. Worth, TX, 2006.
- [20] Phanomchoeng, G., D. Gebre-Egziabher and J. H. Rife, "A Numerical Procedure for Approximating Overbounds on Navigation Systems Error Distributions," *Proceedings of ION-GNSS 2006*, Ft. Worth, TX, 2006.
- [21] Bevely, D., D. Gebre-Egziabher and B. W. Parkinson, "Parametric Error Equations for Dead Reckoning Navigators used in Ground Vehicle Guidance and Control," *Navigation*. Vol. 53, No. 2. pp. 135 - 148.
- [22] Jung, D. and Levy E. J., "Design and Development of a Low-Cost Test-Bed for Undergraduate Education in UAVs," *Proceeding of the European Control Conference 2005*, Seville, Spain, December 12-15, 2005, pp. 2739-2744
- [23] Shao, Y. and D. Gebre-Egziabher, "Stochastic and Geometric Observability of Aided Inertial Navigators," *Proceedings of the ION-GNSS 2006 Conference*, Ft. Worth, TX, 2006.
- [24] IEEE Gyro and Accelerometer Panel, IEEE Std 952-1997, *IEEE Standard Specification Format Guide and Test Procedure for Single-Axis Interferometric Fibre Optic Gyros*,
- [25] Roumeliotis, S. I., *Circumventing Dynamic Modeling: Evaluation of the Error-State Kalman Filter Applied to Mobile Robot Localization*, *Proceedings of the 1999 IEEE, International Conference on Robotics and Automation*, Detroit, Michigan, May 1999, pp. 1656-1663
- [26] Wang, L. and S. Xiong, "Constrained Filtering Method for MAV Attitude Determination," *IMTC 2005, Instrumentation and Measurement Technology Conference*, Ottawa, Canada, 17-19 May 2005, pp. 1480-1483
- [27] Gebre-Egziabher, D., *Design and Performance Analysis of a Low-Cost Aided-Dead Reckoning Navigation System*. Ph.D. Thesis, Department of Aeronautics and Astronautics, Stanford University, Stanford, CA. December 2001. pp. 68-90.
- [28] Gebre-Egziabher, D., R. C. Hayward and J. D. Powell, "Design of Multi-Sensor Attitude Determination Systems," *IEEE Journal of Aerospace Electronic Systems*, Vol. 40, No. 2, 2004. pp. 627 - 643.
- [29] Wenger, L. and Gebre-Egziabher, D., "System Concepts and Observability Analysis of Multi-Sensor Navigation Systems for UAV Applications," AIAA Paper 2003-6647 in *Proceedings of the 2nd AIAA "Unmanned Unlimited" Conference*, San Diego, California, Sep. 15-18, 2003.
- [30] Lim, H. L., B. Newstrom, C. Shankwitz and M. Donath, A Conformal Augmented Heads Up Display for Driving under Low Visibility Conditions, *Proceedings of the 5th International Symposium on Advanced Vehicle Control*, Ann Arbor, MI, August, 2000.

- [31] Alexander, L. P. M. Cheng, M. Donath, A. Gorjestani, B. Newstrom, C. Shankwitz, and W. Trach, Jr., DGPS-based Lane Assist System for Transit Buses, *Proceedings of the 2004 IEEE ITS Conference (ITSC 2004)*, Washington, DC, October 2004.
- [32] Gorjestani, A. , L. Alexander, B. Newstrom, P.M. Cheng, M. Sergi, C. Shankwitz, and M. Donath, *Driver Assistive Systems for Snowplows*, Minnesota Department of Transportation (MnDOT) Report No. 2003-13, March 2003.
- [33] Crossbow Inc., *Specification Sheet for the μ Nav Navigation & Servo Control Board*, Document No. 6020-0083-02, Rev. B. 2006.
- [34] Microbotics Inc., *MIDG II Specifications*, Microbotics Inc., Hampton, VA, USA. August, 2005.
- [35] Stengel, R. F., *Optimal Control and Estimation*. Dover, New York, New York. 1994. pp. 392 – 407.
- [36] Gelb, A., *Applied Optimal Estimation*. The MIT Press, Cambridge, Massachusetts. 1974.
- [37] Brown, G. and P. Y. C. Hwang, *Introduction to Random Signals and Applied Kalman Filtering*, 2nd Edition, John Wiley, New York, New York. 1992.
- [38] Xsens Technologies, *MT9 Inertial 3D Motion Tracker Specification Sheet*, Xsens Technologies, B.V., Enschede, Netherlands.
- [39] Cloud Cap Technology, *Crista Inertial Measurement Unit, Interface/Operation Document*, Cloud Cap Technology Inc., Hood River, OR, USA.